

**SYNTHESIS AND CHARACTERIZATION OF CuS  
BY LASER-ASSISTED SPRAY PYROLYSIS  
DEPOSITION FOR pH SENSOR APPLICATION**

by

**FAYROZ ARIF SABAH ALZUHAYRE**

**Thesis submitted in fulfillment of the requirements  
for the degree of  
Doctor of Philosophy**

**November 2017**

## **ACKNOWLEDGEMENT**

I endured easy and difficult, good and thought provoking times in the course of this research, hence I would like to thank Allah Almighty for His mercy, bounty and for granting me health, patience and the will power to satisfactorily carry out this research. My utmost gratitude to my main supervisor Dr. Naser Mahmoud Ahmed, for his thoughtful insights, motivation and guidance throughout my program. My appreciation for his support, encouragement and inspiring guidance. My gratitude and appreciation also goes to my co-supervisor Prof. Zainuriah Hassan, for her support, concern and assistance in ensuring the completion of my research. My gratitude also goes to Prof. Abdul Razak Ibrahim for his immense assistance.

I also use this medium to appreciate my beloved mother, father, sisters, brother and sister's family for their continual support and prayers. I am forever grateful for their patience, concern, care, love and material and moral support. My gratitude also goes to the staff of School of Physics, NOR lab, solid state lab and the FESEM lab staff at the School of Biological Science-USM, for their enormous assistance. Much of this work would be incomplete without their technical support. My appreciation and gratitude to all my friends and colleagues, thank you for your assistance and support.

Fayroz Arif Sabah

USM, Malaysia 2017

## TABLE OF CONTENTS

<b>ACKNOWLEDGEMENT .....</b>	<b>ii</b>
<b>TABLE OF CONTENTS .....</b>	<b>iii</b>
<b>LIST OF TABLES .....</b>	<b>vii</b>
<b>LIST OF FIGURES .....</b>	<b>ix</b>
<b>LIST OF ABBREVIATIONS .....</b>	<b>xiv</b>
<b>LIST OF SYMBOLS .....</b>	<b>xvi</b>
<b>ABSTRAK .....</b>	<b>xviii</b>
<b>ABSTRACT.....</b>	<b>xx</b>
<b>CHAPTER 1: INTRODUCTION .....</b>	<b>1</b>
1.1 Overview .....	1
1.2 Problem statement .....	3
1.3 Aim of the study .....	4
1.4 Objectives of the study .....	4
1.5 Originality of the study .....	5
1.6 Scope of study .....	5
1.7 Outline of the thesis.....	6
<b>CHAPTER 2: BACKGROUND AND LITERATURE REVIEW .....</b>	<b>7</b>
2.1 Spray pyrolysis deposition .....	7
2.2 CuS overview .....	8
2.3 Thin film deposition using laser beam .....	11

2.4	CuS as a pH sensor material.....	11
2.5	CuS structure .....	14
2.6	Metal oxide semiconductor field effect transistor (MOSFET) structure and operation .....	16
2.7	EGFET as pH sensor device.....	20
2.8	Hysteresis of the pH sensor .....	28
2.9	Conditions and parameters affecting the pH sensitivity.....	29
2.9.1	Influence of thin film material and annealing time .....	29
2.9.2	Influence of high intensity white light and dark on the sensitivity.....	30
2.9.3	Effect of thin film thickness .....	32
2.9.4	Effect of thin film conductivity .....	33
2.9.5	Effect of precursor's solvent .....	34
2.9.6	The role of crystal orientation .....	34
2.9.7	Influence of MOSFET presence and absence on pH sensitivity.....	35
<b>CHAPTER 3: RESEARCH METHODOLOGY AND SPRAY PYROLYSIS DEPOSITION SYSTEM.....</b>		<b>36</b>
3.1	Spray pyrolysis deposition (SPD) .....	37
3.2	Cleaning process of substrates .....	40
3.2.1	Glass substrate .....	40
3.2.2	Silicon substrate.....	40
3.3	Preparation CuS solution for deposition .....	41
3.4	Device fabrication .....	42
3.4.1	pH sensor device.....	42
3.5	Instrumentations .....	44

**CHAPTER 4: RESULTS OF CuS THIN FILMS SYNTHESIZED BY  
SPRAY PYROLYSIS DEPOSITION AND THEIR APPLICATION  
AS pH SENSORS..... 50**

4.1	Introduction .....	50
4.1.1	Precursor's concentration .....	50
4.1.2	Molar ratio of (Cu:S) .....	54
4.1.3	Deposition temperature .....	59
4.1.4	Solvent ratio.....	63
4.2	CuS as a pH sensor.....	66
4.2.1	The role of the sensor material in the pH sensing characteristics .....	66
4.2.2	Effect of annealing time in the sensor conductivity and sensitivity.....	72
4.2.3	Sensitivity measurement in dark and under high intensity white light.....	81
4.2.4	Effect of thin film thickness and precursor's solvent in the sensitivity.....	85
4.2.5	Influence of the crystal orientation on the sensor behaviour.....	91
4.2.6	Effect of MOSFET in pH sensing .....	99

**CHAPTER 5: RESULTS OF CuS THIN FILMS SYNTHESIZED BY  
LASER-ASSISTED SPRAY PYROLYSIS & PHOTOLYSIS  
DEPOSITION ..... 103**

5.1	Introduction .....	103
5.2	Membrane Synthesise .....	103
5.2.1	Laser-assisted spray pyrolysis system .....	103
5.2.2	Laser-assisted spray photolysis system .....	106
5.3	Results and Discussion.....	109
5.3.1	Laser-assisted spray pyrolysis system .....	109
5.3.1(a)	Structural Analysis .....	109

5.3.1(b) Morphological Characteristics .....	110
5.3.1(c) Membrane Roughness .....	112
5.3.1(d) Contact Angle.....	112
5.3.1(e) Electrical Characteristics .....	114
5.3.1(f) pH Sensitivity and Linearity .....	114
5.3.1(g) Hysteresis .....	119
5.3.1(h) Repeatability.....	120
5.3.1(i) Stability & Reliability .....	121
5.3.2 Laser-assisted spray photolysis system .....	123
5.3.2(a) Structural, Morphological, Contact Angle & Electrical Characteristics .....	123
5.3.2(b) pH Sensing Characteristics.....	126
<b>CHAPTER 6: CONCLUSION &amp; FUTURE WORK .....</b>	<b>134</b>
6.1 Conclusion.....	134
6.2 Future Work .....	135
<b>REFERENCES .....</b>	<b>136</b>

**LIST OF PUBLICATIONS**

## LIST OF TABLES

	<b>Page</b>
Table 2.1 Studies of synthesis CuS thin films by spray pyrolysis deposition in literature with different parameters. ....	8
Table 2.2 Studies of synthesis CuS thin films by various deposition methods in literature. ....	10
Table 2.3 Studies of thin film deposition by laser infrared radiation in literature. ....	11
Table 2.4 pH sensors and their properties in literature. ....	12
Table 4.1 Surface roughness of CuS thin films for different precursor's concentration. ....	53
Table 4.2 Electrical parameters of CuS thin films with different precursor's concentration. ....	54
Table 4.3 Surface roughness of CuS thin films with different (Cu:S) molar ratios. ....	58
Table 4.4 Electrical parameters of CuS thin films with different (Cu:S) molar ratios. ....	59
Table 4.5 Surface roughness of CuS thin films with different deposition temperatures. ....	62
Table 4.6 Electrical parameters of CuS thin films synthesized at different deposition temperature. ....	62
Table 4.7 Surface roughness of CuS thin films with different solvent ratio. ....	65
Table 4.8 Electrical parameters of CuS thin films synthesized at different (DIW:Et) solvent ratio. ....	66
Table 4.9 CuS membranes' characteristics without and with annealing at 150 °C. ....	75

Table 4.10	pH characteristics of sensitive membranes under different light conditions.....	85
Table 4.11	pH sensitivity of CuS/ (glass, ITO, Si and tungsten) sensors. ....	96
Table 4.12	pH sensing characteristics of CuS/ (glass, ITO, Si and tungsten) sensors.....	98
Table 4.13	pH sensing characteristics of CuS sensors under various parameters and conditions. ....	102
Table 5.1	Structural & morphological parameters of CuS thin films synthesized by pyrolysis process. ....	113
Table 5.2	Electrical parameters of CuS thin films synthesized by pyrolysis process. ....	114
Table 5.3	pH sensitivity and linearity of CuS thin films synthesized by pyrolysis process.....	123
Table 5.4	Structural, morphological, Electrical and pH sensing characteristics of CuS thin film synthesized by photolysis process. ....	130
Table 5.5	pH sensing characteristics of all CuS/glass sensors that obtained in this study.....	131
Table 5.6	Comparison of pH sensitivity for CuS in this work and other sensing membranes.....	132



## LIST OF FIGURES

	<b>Page</b>
Figure 2.1 Schematic diagram of the covellite (CuS) structure orthogonal with the c-axis. Copper and sulphur ions represented by black and gray spheres, respectively [73].....	15
Figure 2.2 Schematic of n-channel MOSFET [76]. .....	17
Figure 2.3 The accumulation of positive and negative ions in the gate area of the MOSFET. ....	18
Figure 2.4 I-V characteristics and output plot of an n-channel MOSFET [79]. ....	20
Figure 2.5 Schematic model of the electrical double-layer (EDL) at the sensor-electrolyte interface, illustrating the elements of the Gouy-Chapman-Stern model such as; specifically absorbed anions and nonspecifically adsorbed solvated cations [86]. .....	25
Figure 3.1 Experimental procedures flowchart. ....	37
Figure 3.2 (a) Spray system image (b) block diagram of the system. ....	39
Figure 3.3 Precursors and CuS solutions. ....	41
Figure 3.4 pH sensor system (a) A schematic diagram for measuring (I-V) and (I-T) characteristics (b) schematic diagram for measuring (V-T) characteristics (c) image. ....	44
Figure 4.1 XRD patterns of CuS thin films for different precursor's concentration. ....	51
Figure 4.2 FESEM with EDX images of CuS thin films for (a) 0.1 M concentration (b) 0.2 M concentration (c) 0.4 M concentration. ....	52
Figure 4.3 XRD patterns of CuS thin films for (Cu:S) molar ratios (a) (1:2) (b) (1:3). ....	55

Figure 4.4	FESEM with EDX images of CuS thin films with (1:2) molar ratio for (a) 0.1 M concentration (b) 0.2 M concentration (c) 0.4 M concentration.....	56
Figure 4.5	FESEM with EDX images of CuS thin films with (1:3) molar ratio for (a) 0.1 M concentration (b) 0.2 M concentration (c) 0.4 M concentration.....	58
Figure 4.6	XRD patterns of CuS thin films synthesized at different deposition temperature. ....	60
Figure 4.7	FESEM with EDX images of CuS thin films synthesized at (a) 100 °C (b) 300 °C deposition temperature. ....	61
Figure 4.8	XRD patterns of CuS thin films prepared with different (DIW:Et) solvent ratio.....	63
Figure 4.9	FESEM with EDX images of CuS thin films prepared with (DIW:Et) solvent ratios (a) (7:3) (b) (1:4) (c) Ethanol. ....	65
Figure 4.10	Output characteristics ( $I_{ds}$ - $V_{ds}$ ) & ( $I_{ds}$ - $V_{gs}$ ) in saturation and linear regime, respectively of CuS membrane. ....	67
Figure 4.11	Sensitivity and linearity in saturation and linear regime, respectively of CuS membrane. ....	68
Figure 4.12	Hysteresis (delay in pH response) of CuS membrane. ....	70
Figure 4.13	Repeatability in term of (C.V.) for pH7 of CuS membrane. ....	71
Figure 4.14	Stability and reliability in term of (C.V.) for pH 4, pH 7 and pH 10 of CuS membrane. ....	71
Figure 4.15	XRD image of CuS membranes annealed at different annealing time. ....	72
Figure 4.16	FESEM images of CuS membranes (a) without annealing (b-d) annealing at 150 °C for 5, 15 and 30 min. respectively. ....	74

Figure 4.17	( $I_{ds}$ - $V_{ds}$ ) and ( $I_{ds}$ - $V_{gs}$ ) curves of CuS membranes (a) without annealing (b-d) annealing at 150 °C for 5, 15 and 30 min. respectively. ....	77
Figure 4.18	Sensitivity of CuS membranes (a) without annealing (b-d) annealing at 150 °C for 5, 15 and 30 min. respectively. ....	78
Figure 4.19	Sensitivity of CuS membranes with annealing time. ....	79
Figure 4.20	Hysteresis of CuS membranes (a) without annealing (b-d) annealing at 150 °C for 5, 15 and 30 min. respectively. ....	80
Figure 4.21	Repeatability, stability & reliability of CuS membranes (a) without annealing (b-d) annealing at 150 °C for 5, 15 and 30 min. respectively. ....	81
Figure 4.22	( $I_{ds}$ - $V_{ds}$ ) & ( $I_{ds}$ - $V_{gs}$ ) curves of saturation and linear regime, respectively in (a) light source (b) dark. ....	82
Figure 4.23	Sensitivity and linearity for saturation and linear regime, respectively in (a) light source (b) dark. ....	83
Figure 4.24	Hysteresis and drift at buffer solutions of pH (4, 7 and 10) under (a) light source (b) dark. ....	85
Figure 4.25	XRD images of CuS thin film with (a) 4.27 $\mu\text{m}$ thickness (b) 3.59 $\mu\text{m}$ thickness. ....	86
Figure 4.26	FESEM images of CuS thin film with (a) 4.27 $\mu\text{m}$ thickness (b) 3.59 $\mu\text{m}$ thickness. ....	87
Figure 4.27	Output characteristics of CuS EGFET pH sensor with (a) 4.27 $\mu\text{m}$ thickness (b) 3.59 $\mu\text{m}$ thickness. ....	88
Figure 4.28	Sensitivity of CuS EGFET pH sensor with (a) 4.27 $\mu\text{m}$ thickness (b) 3.59 $\mu\text{m}$ thickness. ....	89
Figure 4.29	Hysteresis of CuS EGFET pH sensor with (a) 4.27 $\mu\text{m}$ thickness (b) 3.59 $\mu\text{m}$ thickness. ....	89

Figure 4.30	Repeatability of CuS EGFET pH sensor with (a) 4.27 $\mu\text{m}$ thickness (b) 3.59 $\mu\text{m}$ thickness.....	90
Figure 4.31	Stability and reliability of CuS EGFET pH sensor with (a) 4.27 $\mu\text{m}$ thickness (b) 3.59 $\mu\text{m}$ thickness.....	91
Figure 4.32	Structural characteristic of (a) CuS/ITO thin film (b) CuS/ Si thin film (c) CuS/Tungsten thin film.....	92
Figure 4.33	Morphological characteristic of (a) CuS/ITO thin film (b) CuS/ Si thin film (c) CuS/Tungsten thin film. ....	93
Figure 4.34	Output characteristics (I-V) of (a) CuS/ITO thin film (b) CuS/ Si thin film (c) CuS/Tungsten thin film. ....	94
Figure 4.35	Sensitivity and linearity of (a) CuS/ITO thin film (b) CuS/ Si thin film (c) CuS/Tungsten thin film.....	95
Figure 4.36	Hysteresis (delay in pH response) of (a) CuS/ITO thin film (b) CuS/ Si thin film (c) CuS/Tungsten thin film. ....	96
Figure 4.37	Repeatability as (C.V.) for pH7 of (a) CuS/ITO thin film (b) CuS/ Si thin film (c) CuS/Tungsten thin film. ....	97
Figure 4.38	Stability and reliability as (C.V.) for pH 4, pH 7 and pH 10 of (a) CuS/ITO thin film (b) CuS/ Si thin film (c) CuS/Tungsten thin film.....	98
Figure 4.39	pH sensing behaviour of CuS membrane (a) with MOSFET (b) without MOSFET. ....	101
Figure 4.40	Hysteresis of CuS membrane.....	101
Figure 5.1	(a) Block diagram of laser-assisted pyrolysis system (b) image of the system. ....	105
Figure 5.2	CuS thin films synthesized by laser-assisted spray pyrolysis deposition.....	106

Figure 5.3	(a) Block diagram of laser-assisted photolysis system (b) image of the system. ....	108
Figure 5.4	CuS thin films synthesized by laser-assisted spray photolysis deposition.....	108
Figure 5.5	XRD images of CuS thin films deposited on different substrates by pyrolysis process.....	110
Figure 5.6	FESEM images of CuS thin films deposited by pyrolysis process onto (a) glass (b) ITO (c) Si (d) tungsten substrates.....	111
Figure 5.7	Contact angle of CuS thin films deposited by pyrolysis process onto (a) glass (b) ITO (c) Si (d) tungsten substrates.....	113
Figure 5.8	(current-voltage) characteristics of CuS sensors synthesized by pyrolysis process onto (a) glass (b) ITO (c) Si (d) tungsten substrates.....	116
Figure 5.9	pH sensitivity vs. pH value of CuS sensors synthesized by pyrolysis process onto (a) glass (b) ITO (c) Si (d) tungsten substrates.....	117
Figure 5.10	Hysteresis of CuS sensors synthesized by pyrolysis process onto (a) glass (b) ITO (c) Si (d) tungsten substrates.....	120
Figure 5.11	Repeatability of CuS sensors synthesized by pyrolysis process onto (a) glass (b) ITO (c) Si (d) tungsten substrates.....	121
Figure 5.12	Stability & Reliability of CuS sensors synthesized by pyrolysis process onto (a) glass (b) ITO (c) Si (d) tungsten substrates.....	122
Figure 5.13	Structural and morphological characteristics of CuS/glass thin film deposited by photolysis process (a) XRD (b) FESEM (c) contact angle images. ....	125
Figure 5.14	pH sensing characteristics of CuS/glass sensor synthesized by photolysis process (a) (I-V) characteristics (b) pH sensitivity (c) hysteresis (d) repeatability (e) stability & reliability. ....	128

## LIST OF ABBREVIATIONS

AFM	Atomic force microscopy
ALD	Atomic layer deposition
BGM	Blood glucose monitoring
CBD	Chemical bath deposition
CMOS	Complementary metal oxide semiconductor
CNT	Carbon-nanotube
C.V.	Coefficient of variation
CVR	Chemical vapor reaction
CW	Continuous wave
D	Drain
D.C.	Direct current
DIW	Deionized water
DTO	Dithiooxamide
EDL	Electrical double-layer
EGFET	Extended gate field effect transistor
Et	Ethanol
FESEM	Field emission scanning electron microscopy
FET	Field effect transistor
G	Gate electrode
IFCT	Interfacial charge transfer
ISFET	Ion sensitive field effect transistor
MOD	Metal organic deposition
MOS	Metal oxide semiconductor
MOSFET	Metal oxide semiconductor field effect transistor

MWCNTs	Multiwalled carbon nanotubes
PE	Polyethylene
PET	Polyethylene terephthalate
pH	Power of hydrogen
PLD	Pulsed laser deposition
PVD	Physical vapor deposition
RCA	Radio Corporation of America
RF	Radio frequency
S	Source
SGT	Solution growth technique
SILAR	Successive ionic layer adsorption and reaction method
SPD	Spray pyrolysis deposition
TC	Temperature coefficient
XRD	X-ray diffraction

## LIST OF SYMBOLS

$A$	Area of the thin film
$\beta$	Sensitivity parameter
$^{\circ}C$	Celsius temperature
$C_{DL}$	Capacitance of the electrical double layer
$E_{REF}$	Reference electrode potential
$\psi$	Surface potential voltage
$\varphi_o$	Potential on the gate
$[H^+]_b$	Bulk activity of H <sup>+</sup> ions
$[H^+]_s$	Surface activity of H <sup>+</sup> ions
$I_{ds}$	Drain-source current
$k$	Boltzmann constant
$K_a$	Acidic constant
$K_b$	Basic constant
$K_n$	Conduction parameter
$m$	Mass of the thin film
$\mu_H$	Hall mobility
$N_S$	Total number of surface sites per unit area
$\rho$	Mass of the thin film
$\rho_s$	Room temperature resistivity of the thin film
$p$	Carrier concentration
$pH_{PZC}$	pH value at the point of zero charge
$q$	Electron charge
$R_H$	Hall coefficient
$S$	Sensitivity



$t$	Thickness of the thin film
$T$	Absolute temperature
$V_{ds}$	Drain-source voltage
$V_{gs}$	Gate-source voltage
$V_{REF}$	Reference electrode voltage
$V_{SENSING-FILM}$	Sensing film voltage
$V_{th}$	Threshold voltage
$\Delta B$	Change in the magnetic field
$\Delta R$	Change in the resistance
$\Delta V$	Variable potential between bulk solution and the surface of the film
$g_{nd}$	Ground

# **SINTESIS DAN PENCIRIAN CuS DENGAN PEMENDAPAN PIROLISIS SEMBURAN BERBANTUKAN LASER UNTUK APLIKASI PENGESAN pH**

## **ABSTRAK**

Kajian ini melibatkan aplikasi novel filem kuprum sulfida (CuS) sebagai pengesan pH. Filem nipis CuS yang disintesis digunakan sebagai transistor kesan medan get tambahan (EGFET), yang kemudiannya digunakan sebagai pengesan pH. Kepekaan pH, histerisis, kebolehulangan, kestabilan dan kebolehharian filem nipis CuS diukur. Kesan bahan filem nipis, suhu, pencahayaan, ketebalan pengesan pH, kekonduksian pengesan, struktur permukaan pengesan, jenis larutan prekursor ke atas orientasi kristal dan transistor pancaran medan logam oksida semikonduktor (MOSFET) telah dikaji. Filem nipis CuS telah disintesis atas beberapa substrat menggunakan pirolisis semburan dan pemendapan semburan berbantuan laser pada suhu substrat 200°C. Dua kaedah semburan berbantuan laser telah dijalankan buat pertama kali menggunakan alur laser gelombang berterusan (CW) CO<sub>2</sub> sebagai sumber tenaga; pemendapan semburan pirolisis berbantuan laser yang melibatkan penggunaan tenaga laser untuk memanaskan substrat, dan proses fotolisis semburan berbantuan laser yang berasaskan penyerapan resonans laser CO<sub>2</sub> oleh aerosol. Dalam proses pirolisis, substrat dipasang pada pemegang berputar (kipas) untuk mengurangkan pembentukan lubang dan bagi memastikan pengagihan homogen suhu alur dan larutan yang disembur, manakala substrat dalam proses fotolisis telah diletakkan di atas pemanas (plat panas) dan alur laser tertumpu hanya di hujung aerosol selepas meninggalkan muncung untuk menjamin pengujaan fotolitik. Prekursor kuprum klorida (CuCl<sub>2</sub>·2H<sub>2</sub>O) dan sodium tiosulfat (Na<sub>2</sub>S<sub>2</sub>O<sub>3</sub>·5H<sub>2</sub>O) telah digunakan sebagai sumber Cu<sup>2+</sup> dan S<sup>2-</sup>, masing-masing. Nisbah kepekatan dan

molar daripada prekursor, suhu substrat, jenis pelarut, ketebalan filem nipis, dan jenis substrat telah diubahsuai untuk mencapai objektif kajian ini. Ciri-ciri struktur, morfologi, elektrik dan fizikal daripada filem nipis yang disintesis dianalisis dengan menggunakan meter belauan sinar-X (XRD), mikroskopi imbasan elektron pancaran medan (FESEM), mikroskopi daya atomik (AFM) dan kesan Hall. Ciri-ciri struktur dan morfologi terbaik; Orientasi kristal CuS (006) + atom sulfur di permukaan, ketebalan filem bernilai 2.37 mikron, kekasaran permukaan filem bernilai 0.152 nm, sudut sentuhan permukaan bernilai 18.75°, dan ciri-ciri pengesanan pH tertinggi telah dicapai untuk pengesanan CuS yang disintesis oleh pemendapan fotolisis semburan berbantuan laser; kepekaan pH bernilai 40 mV/pH, histerisis bernilai 0.53 mV, kebolehlungan bernilai 0.04%, dan kestabilan dan kebolehharian bernilai 0.13, 0.19 dan 0.57% masing-masing bagi pH 4,7 dan 10.

# **SYNTHESIS AND CHARACTERIZATION OF CuS BY LASER-ASSISTED SPRAY PYROLYSIS DEPOSITION FOR pH SENSOR APPLICATION**

## **ABSTRACT**

This study involves the novel application of copper sulphide (CuS) films as pH sensors. The synthesized CuS thin films were used as extended gate field effect transistor (EGFET), which was then applied as a pH sensor. The pH sensitivity, hysteresis, repeatability, stability and reliability of the CuS thin films were measured. The effects of thin film material, temperature, illumination, pH sensor thickness, sensor conductivity, sensor surface structure, precursor solvent type on crystal orientation and Metal oxide semiconductor field effect transistor (MOSFET) were studied. The CuS thin films were synthesized on several substrates using spray pyrolysis and laser-assisted spray deposition at substrate temperature of 200°C. Two laser-assisted spray methods were carried out for the first time using continuous wave (CW) CO<sub>2</sub> laser beam as an energy source; laser-assisted spray pyrolysis deposition involving the use of laser energy to heat up the substrate, and laser-assisted spray photolysis process which is based on the resonant absorption of CO<sub>2</sub> laser by aerosols. In the pyrolysis process, the substrate was mounted on a rotating holder (fan) to minimize pit formation and to ensure homogeneous distribution of beam temperature and sprayed solution, while the substrate in photolysis process was positioned on a heater (hot plate) and the laser beam was focused just on the aerosols tip after leaving nozzle to guarantee photolytic excitation. Copper chloride (CuCl<sub>2</sub>·2H<sub>2</sub>O) and sodium thiosulfate (Na<sub>2</sub>S<sub>2</sub>O<sub>3</sub>·5H<sub>2</sub>O) precursors were used as Cu<sup>2+</sup> and S<sup>2-</sup> sources, respectively. The concentration and molar ratio of the precursors, substrate temperature, solvent type, thin film thickness, and substrate type were

modified to achieve the objectives of this study. Structural, morphological, electrical and physical characteristics of the synthesized thin films were analyzed using X-ray diffractometer (XRD), field emission scanning electron microscopy (FESEM), atomic force microscopy (AFM) and Hall effect. The best structural and morphological features; CuS crystal orientation (006) + sulphur atoms at the surface, film thickness of 2.37  $\mu\text{m}$ , film surface roughness of 0.152 nm, surface contact angle of 18.75°, and the highest pH sensing characteristics were achieved for CuS sensor synthesized by laser-assisted spray photolysis deposition; pH sensitivity of 40 mV/pH, hysteresis of 0.53 mV, repeatability of 0.04%, and stability and reliability of 0.13, 0.19 and 0.57% for pH 4,7 and 10, respectively.

## CHAPTER 1: INTRODUCTION

### 1.1 Overview

The structural, optical and electrical properties of Copper sulphide (CuS) has been investigated in bulk and single crystals as well as thin film forms. These properties are largely controlled by the local chemical composition of CuS, which is found to be strongly dependent on the preparation technique and the deposition conditions that prevail during crystal growth. CuS thin film has garnered a lot of interest because of its exceptional semiconducting properties. In addition, the constituent elements of CuS material (Cu and S) are non-toxic and abundant in nature [1]. Moreover, Copper sulphides ( $\text{Cu}_x\text{S}$ ) are considered important materials to be applied in the manufacture of p-type semiconductors and optoelectronics [2].

Copper and sulfur form a number of phases, four of which are known to be stable at room temperature: covellite (CuS) in the sulfur-rich region, and chalcocite ( $\text{Cu}_2\text{S}$ ), djurlite ( $\text{Cu}_{1.95}\text{S}$ ), and anilite ( $\text{Cu}_{1.75}\text{S}$ ) in the copper-rich region [3]. The covellite phase in the unit cell of CuS is a hexagonal crystal structure. CuS films have high absorption coefficient ranging between  $5 \times 10^4 - 1 \times 10^5 \text{ cm}^{-1}$  in the visible region with effective band gap of  $\sim (2.4 - 2.6 \text{ eV})$  [2, 4]. CuS has a bulk band gap of 2.5 eV [5], while for nanostructured films, the direct bandgap varies significantly (1.26-2.9 eV) [1, 6]. The carrier concentration is in the range of ( $\times 10^{17} / \text{cm}^3$ ) [7]. The water contact angle of CuS thin film is  $44^\circ$ , which indicates a hydrophilic behavior [8].

CuS thin films have been deposited using several techniques that include vacuum evaporation [9], successive ionic layer adsorption and reaction (SILAR) [6],

sol–gel method [10], chemical bath [11] and spray pyrolysis deposition (SPD) [2]. SPD method was selected in this study because of its benefits; comprising cost effectiveness, portability, large effective area coverage with homogenous film, safe to use inside the fume hood, easy to assemble in the lab, and its easily controllable experimental parameters.

The CO<sub>2</sub> laser (10.6 μm) is the most practical molecular laser because of its high level of efficiency and can be produced in continuous wave (CW) and pulse operation [12]. Laser-assisted synthesis can be either pyrolytic or photolytic. The pyrolytic process entails the use of laser energy to heat the substrate (in place of heater), while the photolytic process is based on the resonant absorption of the laser wavelength by aerosols/carrier gases [13]. Some studies have conducted the deposition process via CO<sub>2</sub> laser IR radiation. Zirconium dioxide (ZrO<sub>2</sub>) have been deposited on different substrates; Si, quartz and optically polished glass substrates under different temperatures using CW CO<sub>2</sub> laser-assisted evaporation. Dense optical alumina films have been synthesized using Nd:YAG laser-assisted ultrasonic pyrolysis technique. This pyrolytic or photolytic approach is a new technique for obtaining fine and more concentrated precursor droplets compared to regular spray pyrolysis [14].

Furthermore, Copper sulfide films are commonly used as precursor materials in the manufacture of solar cells, solar control coating, microwave shielding coating, electroconductive electrodes, gas sensor, optical filters, photothermal conversion and electroluminescence [1, 11, 15, 16]. Since the inception of the pH sensor or proton sensor (ion sensitive field effect transistor (ISFET)) by Bergveld in 1970 [17], several modifications have been made. Van der Spiegel et al. [18] conducted the first

study on extended gate field effect transistor (EGFET). pH at room temperature is the power of hydrogen and its range is (0-14), also defined as the negative logarithm of hydrogen ion ( $\text{pH} = -\log [\text{H}^+]$ ). The EGFET comprised sensing membrane and metal oxide semiconductor field effect transistor (MOSFET). The chemically sensitive membrane was synthesized at the end of sole line extended from the FET gate electrode to isolate the FET from the chemical electrolyte [19].

Sensor is referred to as an ‘electronic nose’ that provides an interface between the electronic equipment and the physical world, usually by transforming non-electrical physical or chemical quantities into electrical signals [11]. Given that pH sensing principle is related to surface phenomena, nanocrystalline thin films has attracted a lot of attention. CuS thin films did not perform as pH sensor in literature, therefore, in this study, they applied for the first time as pH sensors.

## **1.2 Problem statement**

The application of CuS thin films synthesized by SPD as a pH sensor is ineffective because it offers low sensitivity due to its structural characteristics. To handle this problem of low pH sensitivity, laser-assisted spray pyrolysis method is proposed. The laser-assisted spray pyrolysis will be used to enhance the crystallinity of the CuS film, reduce the film thickness and increase the sensitivity of the sensor. However, laser-assisted spray pyrolysis has some drawbacks such as; the film deposition is limited to the area of the laser spot (the coating area is limited by the contact zone between laser beam and the substrate) rather than cover all the substrate, which will affect the contact between the film and the electrode of the instrument. In addition, only one thin film can be produced per deposition using laser-assisted spray pyrolysis.



To rectify the drawbacks associated with laser-assisted spray pyrolysis and improve pH sensing characteristics, this study recommends the laser-assisted spray photolysis method. In the laser-assisted spray photolysis method, the laser beam is directed on to the precursor droplet released by the nozzle to ensure photolytic excitation and to provide heat to the solution. Hence, the precursor endures solvent evaporation and solute sublimation, after which coating is achieved via vapor decomposition. This process will likely provide large coating area across all the heater, hence, several thin films can be synthesized at the same time via laser-assisted spray photolysis. Besides, the laser-assisted spray photolysis system is more safe to use than the previous system, because the scattering of laser beam will be prevented by the protective chamber, thus ensuring human safety and non-destruction of instruments or equipment in the lab.

### **1.3 Aim of the study**

The aim of this research study is to improve the structure characteristics of CuS thin film, hence; to enhance its pH sensing characteristics. The structure characteristics improvement was performed by investigated novel deposition method of laser-assisted spray photolysis process, this process provides precursor decomposition that result in presence of sulphur atoms on the film surface to increase the attraction of protons, which leads to increase the CuS thin film sensitivity.

### **1.4 Objectives of the study**

The main objectives of this research study are outlined in the points below:

1- To synthesize CuS thin films using spray pyrolysis deposition on various substrates (glass, ITO, Si and tungsten) under different conditions (precursor's

concentration, molar ratio, deposition temperature and solvent type), and their characteristics then studied.

2- To improve the characteristics of CuS thin films by synthesizing them with Laser-assisted spray pyrolysis and photolysis depositions.

3- To determine the application of the synthesized CuS thin films as pH sensors for different conditions and environments (thin film material, thin film annealing, light, thin film thickness, conductivity, precursor's solvent, crystal orientation, and MOSFET).

### **1.5 Originality of the study**

This is the first study to apply CuS thin films deposited by SPD as pH sensors under different conditions and environments. In addition, the synthesis of CuS thin films by laser-assisted spray pyrolysis and photolysis depositions, and subsequent application as pH membranes is a novel concept.

### **1.6 Scope of study**

This work includes preparation of CuS thin film by means of spray pyrolysis deposition. The synthesized films were then applied as pH sensors. This study also entails the deposition of CuS thin films using CW CO<sub>2</sub> laser based techniques, and they include laser-assisted spray pyrolysis and laser-assisted spray photolysis. The CW CO<sub>2</sub> laser based techniques are expected to compensate for some of the drawbacks of spray pyrolysis, thus enhancing the film characteristics, and improving the pH sensing characteristics.

## **1.7 Outline of the thesis**

This work consists of six chapters. Chapter 1 entails a general synopsis of the work, problem statement, aim of the study, objectives and originality of the thesis. Chapter 2 provides a concise review of CuS thin films, their characteristics, pH sensors, theoretical background of CuS film structure, and pH sensing mechanism. Chapter 3 describes the methodology and the system used for deposition, as well as the instrumentation used to characterize the CuS thin films and pH sensor system. Chapter 4 presents the results of CuS thin film synthesis via spray pyrolysis deposition. The application of these synthesized films as pH sensors is also discussed in this chapter. Chapter 5 focuses on the use of CW CO<sub>2</sub> laser beam for the deposition of CuS thin films through laser-assisted spray pyrolysis and laser-assisted spray photolysis methods, and characterization of the synthesized CuS films and their applications as pH sensors. Chapter 6 presents the conclusions of the study in addition to suggestions for possible future works.

## CHAPTER 2: BACKGROUND AND LITERATURE REVIEW

Previous studies related to CuS thin film and its parameters were concisely reviewed in this chapter. Furthermore, this chapter explains the theoretical concepts of the CuS structure, MOSFET, site-bonding model and EGFET used as pH sensor. These parameters comprise; the selected method of deposition, influence of solvent, precursors' concentrations and molar ratio, substrate type, film thickness and annealing effects. CuS thin films were applied as pH sensors. Detailed literature review showed that CuS has not been previously implemented as this application. Previous studies have only reported the application of CuO [20] rather than CuS thin films as pH sensors. The priority of CuS as a pH sensor belongs to the availability of sulphur atoms on the surface of the film, which attract more protons then result in increasing the pH sensitivity.

### 2.1 Spray pyrolysis deposition

The spray pyrolysis method has been extensively utilized to chemically deposit CuS and other sulfide thin films such as; CdS, ZnS, SnS, PbS, Sn<sub>2</sub>S<sub>3</sub>, etc. [21-25] because this method entails good homogenous deposition, effective adhesion, large treatment area, economical, simple equipment, and portable. CuS thin films have been deposited by spray pyrolysis deposition in numerous studies for different parameters, as listed in Table 2.1. These parameters include; (Cu:S) molar ratio, deposition temperature, precursor's composition, solvent type, spray cycle, the effect of substrate on the film structure, crystal orientation and the CuS phase, furthermore; study the effect of the distance between the nozzle and the substrate.

Table 2.1: Studies of synthesis CuS thin films by spray pyrolysis deposition in literature with different parameters.

Materials	(Cu:S) Molar ratio	Deposition temperature (°C)	Aim of the study	Ref.
CuCl <sub>2</sub> .2H <sub>2</sub> O SC(NH <sub>2</sub> ) <sub>2</sub>	1:5	150-210	Study the effect of different molar ratio	[26]
Thiourea Cu(NO <sub>3</sub> ) <sub>2</sub> .H <sub>2</sub> O	1:1 & 1:5	200-800	Study the effect of precursor composition and temperature of deposition on the particle's crystalline phase	[27]
CuCl <sub>2</sub> .2H <sub>2</sub> O SC(NH <sub>2</sub> ) <sub>2</sub>	-	200-210	Study the effect of the spray cycle, and the distance between the nozzle and substrate on the applicability of CuS thin films as solar cells	[28]
CuCl <sub>2</sub> .2H <sub>2</sub> O SC(NH <sub>2</sub> ) <sub>2</sub>	different molar ratios	185-285	Study the growth of the thin films by increasing alcohol concentration in precursor solution & deposition temperature	[29]
Cu(CH <sub>3</sub> COO) <sub>2</sub> SC(NH <sub>2</sub> ) <sub>2</sub>	0.33 & 0.43	260, 285 & 310	Study optical characteristics and the effective band gap of the films	[4]
Cu(CH <sub>3</sub> COO) <sub>2</sub> SC(NH <sub>2</sub> ) <sub>2</sub>	0.33 & 0.43	285	Study the change of the orientation and CuS phase by changing the substrate	[2]

## 2.2 CuS overview

Copper sulphide (CuS) is a vital semiconductor material because of its conducting properties, band gap energy, multiple structural phases, structural variations, ease of fabrication, inexpensiveness and natural availability, non-toxic nature and eco-friendliness. Copper sulphide is also a viable substitute for many other materials. In view of these exceptional properties, Copper sulphide material has been used in various applications such as the manufacture of solar cell, gas sensors devices, microwave shielding coatings, pH sensors and biosensors, IR detectors, photoconductors, and electrical conductor electrodes [1, 15, 30, 31]. This study is the first to use CuS thin films as pH sensors.

Copper sulphide (CuS) can be deposited by very straightforward, inexpensive and harmless methods such as spray pyrolysis, chemical bath, sol-gel, and so on. The general synthesized structures of CuS thin films include nanoparticles, nanotubes, nanowires, nanoplates and flower-like structure. CuS can be applied as a high-quality electroconductive electrode given its good p-type conductivity. It can also be employed as microwave shielding coatings and solar control coatings based on its good optical features. The quality and behavior of CuS thin film are dependent on several factors that include type of solvent, precursors' concentration and their molar ratios, type of substrate, thin film thickness, annealing duration and temperature of deposition.

Given its exceptional qualities and viability, several studies have been carried out on the synthesis, characteristics and parameters of CuS thin films in order to optimize its applicability. CuS thin films have been synthesized by many different methods such as; spray pyrolysis deposition (SPD) [29], chemical bath deposition (CBD) [30], successive ionic layer adsorption & reaction method (SILAR) [6], Sol-Gel growth [10], atomic layer deposition (ALD) [32], hydrothermal method [33], solution growth technique (SGT) [34], chemical vapor reaction (CVR) [35], and metal organic deposition (MOD) [36]. The main findings of the deposition of CuS thin films in literature were listed in Table 2.2.

Table 2.2: Studies of synthesis CuS thin films by various deposition methods in literature.

Deposition method	Aim of the study	Ref.
SILAR	study the deposition of CuS thin film on different layers comprising CdS buffer layer, glass and ITO substrates. Precursor concentration was found to control the growth rate of CuS thin film.	[37]
SILAR	Deposit CuS thin films onto glass substrates at room temperature. Then study the effect of thin film thickness on the optical and electrical properties, which showed that band gap decreases while the electrical conductivity increases with increasing thickness.	[38]
SILAR	Study the nanostructure characteristics of $(\text{PbS})_x(\text{CuS})_{1-x}$ thin films deposited onto glass substrate at room temperature. The analysis revealed they are characterized by nanocrystalline structure with mixed phase of cubic PbS and hexagonal CuS.	[39]
ALD	Deposit CuS thin films onto glass and Si (100) substrates over temperature ranges of 125-140°C and 125-160°C, respectively. And study the film thickness and resistivity.	[40]
SGT	Study the influence of annealing on the $\text{Cu}_x\text{S}$ thin films at 250°C in Ar atmosphere.	[34]
CBD	Study the thickness and conductivity of CuS thin films deposited onto FTO substrate.	[41]
Vacuum evaporation	Synthesize $\text{Cu}_2\text{S}$ thin films onto glass substrates from CuS powder. And study the annealing effects on the resistivity of the thin films.	[42]
CBD	Study the morphology, thickness and roughness of CuS thin films deposited onto glass substrate.	[43]
MOD	Study the carrier concentration, mobility and resistivity of CuS thin films.	[36]
CBD	Study the effect of annealing effects on the CuS thin films, and the influence of Cu concentration on the optical characteristics.	[44]
CBD	Analyze the effect of copper ion concentrations on the structural and optical properties of CuS thin films deposited onto glass substrate.	[45]
-	Investigate a p-n heterostructure diode composed of CuS/PANI deposited in the hallow network of ZnO thin film deposited onto glass substrate. Then study the optical, electrical characteristics and long-term stability.	[10]

### 2.3 Thin film deposition using laser beam

As mentioned previously, spray pyrolysis depends on temperature to complete the deposition process and to ensure adherence of the synthesized thin film onto the substrate, a heater has been used for the synthesis of CuS thin films. The precursor droplet decomposes to perform nanostructured coatings onto substrates depending on the temperature profile across the reactor and the nature of the precursor. Electric heater or flame is generally providing the energy to pyrolyze [13].

The CO<sub>2</sub> laser is the most practical molecular lasers because of its high level of efficiency and can be produced in continuous wave (CW) and pulse operation. The CO<sub>2</sub> laser 10.6 μm infrared radiation is generated by the energy exchange between rotational-vibrational levels within the electron ground level [12]. The 9-12 μm wavelength of CO<sub>2</sub> laser is useful as it falls into an important window, because many natural and synthetic materials have strong characteristic absorption in this range [46]. Table 2.3 lists few studies for deposition films via laser infrared radiation.

Table 2.3: Studies of thin film deposition by laser infrared radiation in literature.

Deposition method	Aim of the study	Ref.
CW CO <sub>2</sub> laser-assisted evaporation	Deposit zirconium dioxide on various substrates at different temperatures, and study the surface roughness, structure and the crystallinity of the thin film.	[47]
Nd:YAG laser assisted ultrasonic pyrolysis	Synthesis a dense optical alumina films. This approach is a new technique to obtain fine and more concentrated precursor droplets compared to regular spray pyrolysis.	[13]

### 2.4 CuS as a pH sensor material

The application of CuS thin film as a pH sensor was not dealt with in prior research. Therefore, this study applied CuS thin films as pH sensors at different



conditions and factors. Nonetheless, this section reviews the sensitive parameters of other materials that have been deployed as pH sensors under different conditions.

Table 2.4 lists the pH sensors in literature and their properties.

Table 2.4: pH sensors and their properties in literature.

pH sensor	Aim of the study	Ref.
SnO <sub>2</sub> /Si <sub>3</sub> N <sub>4</sub> /SiO <sub>2</sub> /Si	Demonstrate the influence of temperature and light exposure on the sensitivity of the membrane. Study the temperature coefficient (TC) of the interface between thin oxide membrane and electrolyte.	[48]
SnO <sub>2</sub> /aluminium/glass, ITO, SnO <sub>2</sub> /ITO	Analyze five structures of extended gate field effect transistor (EGFET), and study the effect of the contact window on the membrane sensitivity and drift.	[49]
SnO <sub>2</sub>	Study the sensor characteristics when subject to light illumination of 2000 lx.	[50]
TiN	Fabricate the membrane in the same chip with the complementary metal oxide semiconductor (CMOS), and use the amplifier circuit to search for the output voltage.	[51]
ITO	Study the sensing characteristics of the sensor, and the influence of contact window on the sensitivity.	[52]
ITO/Si, ITO/SiO <sub>2</sub> /Si	Study the role of SiO <sub>2</sub> buffer layer in the sensor operation, which prevents or reduce the internal disturbance and interface traps caused by Si.	[53]
IrO <sub>2</sub>	Study the pH sensing characteristics and the deviation of the membrane.	[54]
V <sub>2</sub> O <sub>5</sub> /HDA	Analyze the applicability of the membrane synthesized on glassy carbon substrate as a pH sensor, and suggest that the EGFET structure requires additional number of active sites, in order to increase ion-electrolyte exchange and sensitivity.	[55]
RuN	Study the sensitivity, hysteresis and drift rate at 25°C for solutions in the pH range of 1-13. Also measure the pH sensitivity across different temperatures. The optimum and highest sensitivity was attained at the highest temperature (55°C).	[56]
porous nitrocellulose onto SnO <sub>2</sub> /ITO	Immobilize the urea content of this film and afterwards implemented as a urea biosensor, and study the stability of the sensor. The results confirm the applicability of these films as biosensor in order to determine the presence of enzymes or antigen-antibody reactions. Stability was performed by detecting 27 measurements over 60 days.	[57]

FTO	Validate the applicability of FTO thin films as biosensor device.	[58]
ZnO	Studied the application of ZnO thin films as EGFET in glucose biosensors. This device showed an improvement in sensitivity, which can be attributed to the passivation of dangling bonds and the surfaces of the sidewalls of ZnO nanorods. This confirms that increasing the surface-to-volume ratio will in turn increase the sensitivity of the device.	[59]
ITO/PET	Measure the sensitivity in dark and under light illumination, and study the sheet resistance of the sensor. Also analyze the sensitivity behavior of the thin films at temperatures (25-50°C), the best sensitivity was attained at 40°C.	[60]
V <sub>2</sub> O <sub>5</sub> /WO <sub>3</sub>	Study the use of smaller materials in the EGFET sensor; which is preferred for higher sensitivity. Increasing the volume of the thin films, result in reducing the importance of the changes of surface charges to bulk charges. This reduction will result in less sensitivity and less stability in sensor response.	[61]
CNT	Study the film exposure to CW laser treatment with power of 4 W, the electrical conductivity was improved and the sensitivity increased.	[62]
CuO	Study the surface-to-volume ratio of the film surface and its effects on the pH sensitivity.	[20]
TiN/SiO <sub>2</sub> /Si	Study the effect of the substrate temperature on the pH sensitivity.	[63]
CZTSe	Study the surface-to-volume ratio of the film surface and its effects on the pH sensitivity.	[64]
PdO	Study the ability of the sensor to absorb hydrogen gas at room temperature. The exceptional features of this disposable sensor make it a suitable candidate for economical biochemical sensing. It shows the highest sensitivity compared to other pH sensors.	[65]
InN	Study the surface-to-volume ratio of the film surface and its effects on the pH sensitivity.	[19]
TiO <sub>2</sub> /ITO	Study the effect of annealing time on the pH sensing behaviour of the thin films.	[66]
TiO <sub>2</sub> /ITO	Study the effect of annealing time and the film thickness on the pH sensing behavior of the thin films.	[67]
SnO <sub>2</sub> /ITO	Demonstrate the effect of light illumination on the sensing extended gate.	[68]
Si <sub>3</sub> N <sub>4</sub>	Study the effect of light illumination on sensing membrane.	[69]
TiO <sub>2</sub> /ITO	Study the influence of the thickness of on the sensitivity of the pH sensor.	[70]
WO <sub>3</sub>	Study the sensing characteristics of the sensor, and propose it as a viable candidate for the manufacture of biosensor for urea and glucose detection.	[71]

CuS membrane was applied as a pH sensor in different conditions for the first time, the results of these applications can be found in chapters 4 and 5. The highest pH sensing characteristics were obtained for CuS/glass membrane synthesized by laser-assisted spray photolysis deposition; the pH voltage sensitivity was 40 mV/pH with linearity 97.78%, the pH current sensitivity was 30  $\mu$ A/pH with linearity 98.87%, the hysteresis was 0.53 mV, the repeatability in terms of coefficient of variation (C.V.) at pH7 was 0.04% and the stability & reliability in terms of (C.V.) was 0.13%, 0.19% and 0.57% at pH4, pH7 and pH10, respectively. The pH voltage sensitivity of CuS/glass (40 mV/pH) can be considered acceptable value, it is about 67.57% compared to the standard sensitivity (Nernstian pH sensitivity of 59.2 mV/pH).

## 2.5 CuS structure

Copper sulphides ( $\text{Cu}_x\text{S}$ ) are applied in the manufacture of p-type semiconductors and optoelectronics, solar control coatings, electronic devices, thermal conversion and photovoltaic applications, optical filters, microelectronic devices manufacture and low temperature gas sensor applications. Copper sulphide system ( $\text{Cu}_x\text{S}$ ) has at least five stable phases with ( $1 \leq x \leq 2$ ), which comprises; covellite ( $\text{CuS}$ ), anilite ( $\text{Cu}_{1.75}\text{S}$ ), digenite ( $\text{Cu}_{1.8}\text{S}$ ), djurleite ( $\text{Cu}_{1.97}\text{S}$ ) and chalcocite ( $\text{Cu}_2\text{S}$ ). The structure of covellite phase in the unit cell is a hexagonal crystal structure [72]. As illustrated in Figure 2.1, there are two suitable mediums for both copper and sulphur, which can be expanded into a two-dimensional layer orthogonal with the c-axis. These layers are joined together by sulphur atoms [73].

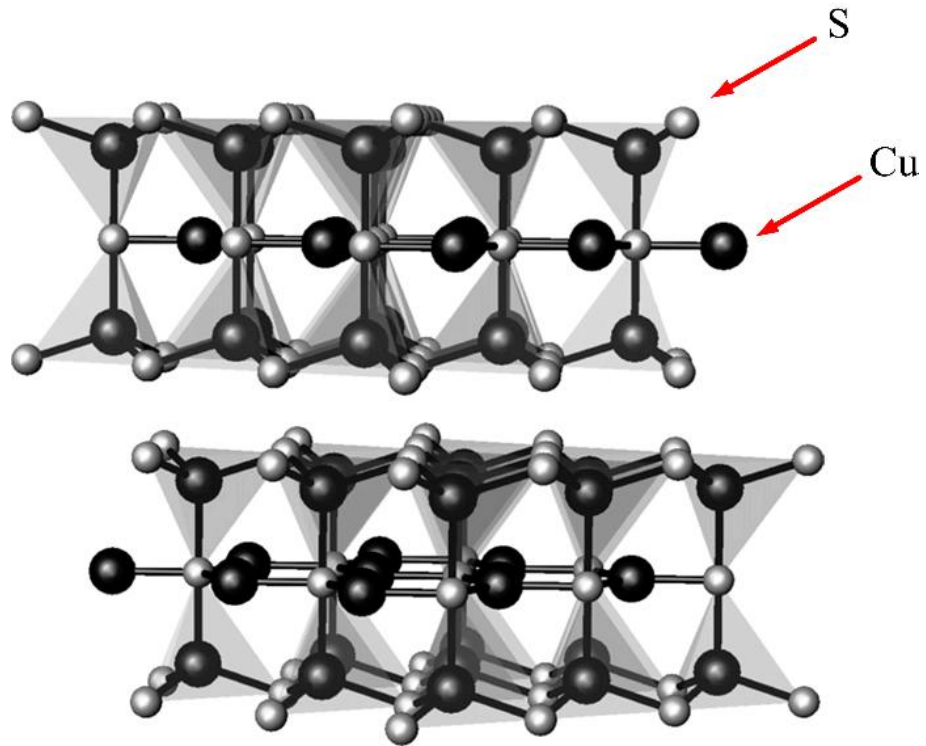


Figure 2.1: Schematic diagram of the covellite (CuS) structure orthogonal with the *c*-axis. Copper and sulphur ions represented by black and gray spheres, respectively [73].

Several methods have been used to synthesize polycrystalline CuS materials of different structures (microstructures and nanostructures). Copper sulphides were synthesized by the reaction of copper with sulphur elements, however, low temperature ( $<150^{\circ}\text{C}$ ) do not help to complete the direct reactions of these elements. Moreover, the reactions are limited to the surface of the copper particles simply because the surface layer of CuS behaves as a passivating layer which prevents further reaction. As posited by Blachnik and Muller [74], a solvent is requisite to complete the reaction and to lower the reaction temperature. In addition, complexing agent will control the morphology of the CuS product, while higher temperature increases the diffusion rate [73].

Tang et al. [75] demonstrated the significant role of solvent and temperature in the synthesis of CuS particles and structures. They show how different arrangements of flake-like CuS crystallites are synthesized from solvothermal reactions. They discovered that the flower-like morphology of CuS nanocrystals can be controlled by solvent as the reaction environment, copper source and reaction time [75].

Numerous materials have been used as the sulphur source, particularly  $\text{Na}_2\text{S}_2\text{O}_3 \cdot 5\text{H}_2\text{O}$ , which is used as an alternative to  $\text{H}_2\text{S}$ , because of its non-toxic nature. These materials can decompose to  $\text{H}_2\text{S}$ , elemental sulphur, or sulphur ions. Micro-crystalline CuS can be synthesized by the reaction of  $\text{Na}_2\text{S}_2\text{O}_3 \cdot 5\text{H}_2\text{O}$  with different copper sources such as;  $\text{CuO}$ ,  $\text{CuSO}_4 \cdot 5\text{H}_2\text{O}$ , and  $\text{CuCl}_2 \cdot 2\text{H}_2\text{O}$  [73].

## **2.6 Metal oxide semiconductor field effect transistor (MOSFET) structure and operation**

A MOSFET is a 2-D device that consists of a p-type substrate, two n-type areas referred to as drain (D) and source (S), and a gate electrode (G) located directly above the p-type zone. The gate electrode is either a metal body or a heavily doped poly-Si layer. Figure 2.2 illustrates the structure and mechanism of the MOSFET. The drain is a high voltage contact while the source is a low voltage contact for MOSFET channel. The input voltage of the MOSFET is applied to the poly-Si gate or metal gate whereas, substrate and source are generally grounded ( $g_{nd}$ ) and at the drain a voltage called drain-to-source voltage ( $V_{ds}$ ) is applied to extract the charge carriers. The drain-to-source current flows through a conducting channel that connects the source zone to the drain zone. The source and drain zones are heavily

doped to decrease the series resistance, thus these two zones provide great volume of electrons to the MOS operation [76].

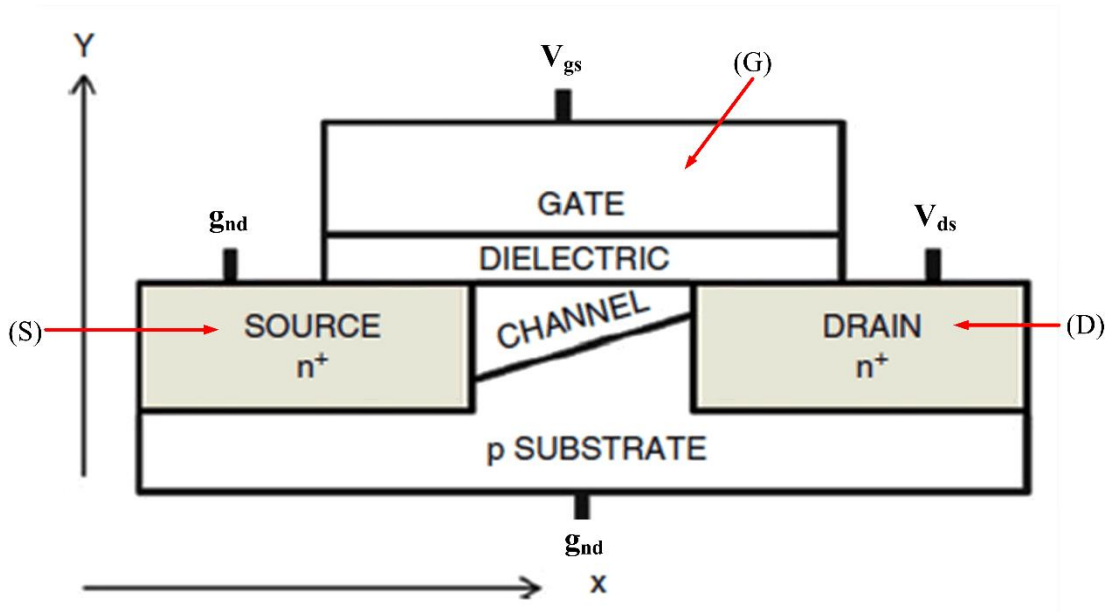


Figure 2.2: Schematic of n-channel MOSFET [76].

The principle of operating the long channel MOSFET depends on applying gate voltage to create electric field at the poly-Si gate through an insulator (normally SiO<sub>2</sub>) to modulate the conductivity of the implied semiconductor. The ideal MOSFET structure has metal gate or a poly-Si gate as mentioned above, the oxide as a perfect insulator (dielectric) with zero tunnelling current and no interface charges, result in the bulk is far from the interface [76].

The mechanism of the MOSFET is in different phases. Firstly, at equilibrium state there is no depletion region, but the application of voltage few electrons near the gate will initiate the depletion region. Afterwards, the conductive channels, source (S) and drain (D), are constructed. The MOSFET determines the flow of electrons from S to D by controlling the morphology (size and shape) of the conductive channel. The channel size in turn controls the positivity or negativity of

the gate-source voltage ( $V_{gs}$ ). In pH sensing application, positivity denotes  $[H^+]$  and negativity means  $[OH^-]$ . The dependency of the conductive channel size on the applied voltage can be attributed to the accumulation of positive voltage at the gate of the MOSFET. This would initiate an increase in the conductive channel with concomitant increase in the current [77]. In contrast, for the accumulation of negative voltage, the conductive channel becomes confined or closed when extra negative voltage is applied, thus decreasing the current as illustrated in Figure 2.3.

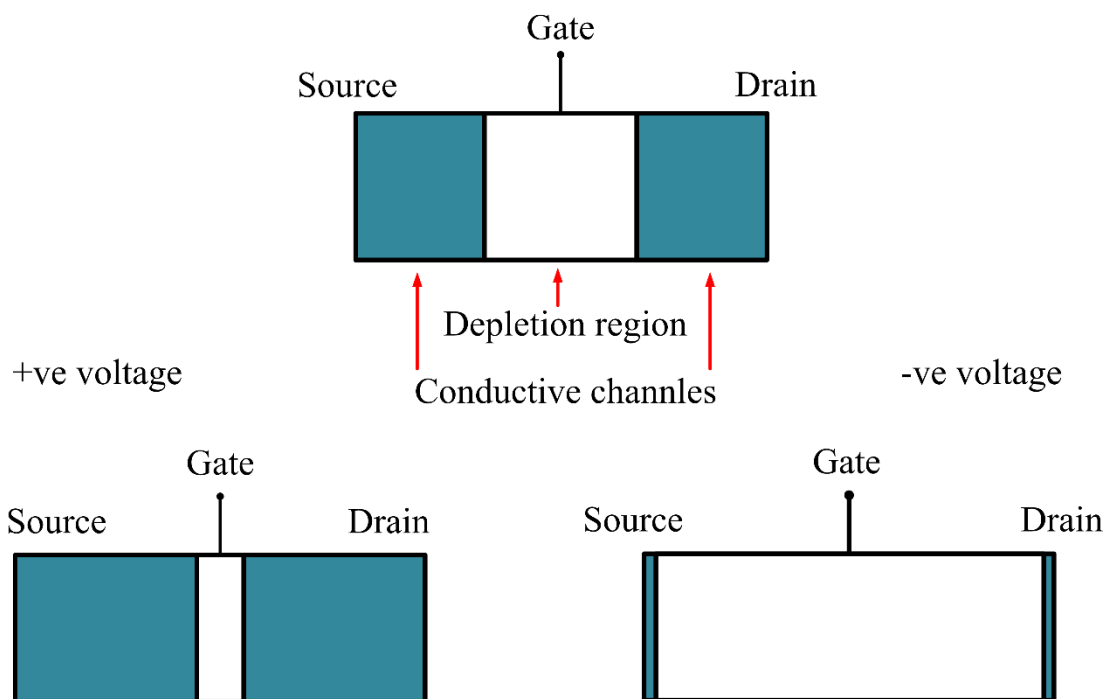


Figure 2.3: The accumulation of positive and negative ions in the gate area of the MOSFET.

The channel region of the silicon MOSFETs is shaped by MOS sandwich to allow alteration of the channel conductivity with application of the gate bias [78]. As the gate-to-source voltage ( $V_{gs}$ ) controls current flow between D and S, the MOSFET gate will be substituted by the extended gate of the field effect transistor to be implemented as a pH sensor. CuS membrane is applied as an extended gate field effect transistor (EGFET) to measure the pH sensitivity. This measurement is

dependent on the accumulation of positive ions  $[H^+]$  (protons) at the gate, where increase in the number of protons subsequently increases the potential voltage of the CuS membrane surface, which in turn improves the ion-exchange process that increases the accumulation of positive charges on the membrane surface (gate region), consequently augmenting the pH sensitivity [77].

The dependency of threshold voltage on the pH value can be illustrated using equation below [68]:

$$[H^+]_s = [H^+]_b \exp(-q\phi_o/kT) \quad (2.1)$$

where  $[H^+]_s$  and  $[H^+]_b$  are the surface and bulk activity of  $H^+$  ions,  $q$  is the electron charge,  $\phi_o$  is the potential on the gate,  $k$  is the Boltzmann constant and  $T$  is the absolute temperature.

In the linear region of the MOSFET, the drain-source current ( $I_{ds}$ ) can be expressed by the below equation [77]:

$$I_{ds} = K_n [2(V_{REF} - V_T)V_{ds} - V_{ds}^2] \quad (2.2)$$

Where  $K_n$  is the conduction parameter.

There are two significant parameters control the MOSFET operation; the carrier concentration in the substrate and the voltage existing in the MOS contacts. This voltage is a kind of an offset voltage, which is applied at the gate so as to cancel the effect of difference in the fermi energies of the metal gate or poly-Si gate and Si substrate. The difference in fermi energy leads to create the electrical field or the potential difference or the band bending in the three materials. To start the device as per our requirement, this band bending has to be overcome. Because of the presence



of oxide there is no flow of charge in MOS structures and only the creation of charge takes place in the two contact materials (gate and substrate). And depending on the polarity of the gate voltage, the MOSFET behaves in three regions; accumulation, depletion and channel creation, as described previously [76].

The I-V characteristics of MOSFET can be illustrated in Figure 2.4, two regimes were recognized (saturation and linear regimes). These curves depend basically on two parameters  $V_{ds}$  and  $V_{gs}$ ; in the saturation regime,  $V_{gs}$  or the voltage of reference electrode ( $V_{ref}$ ) must be constant to plot these curves. While for linear regime,  $V_{ds}$  must be constant and various values of  $V_{gs}$  were used to plot the curves.

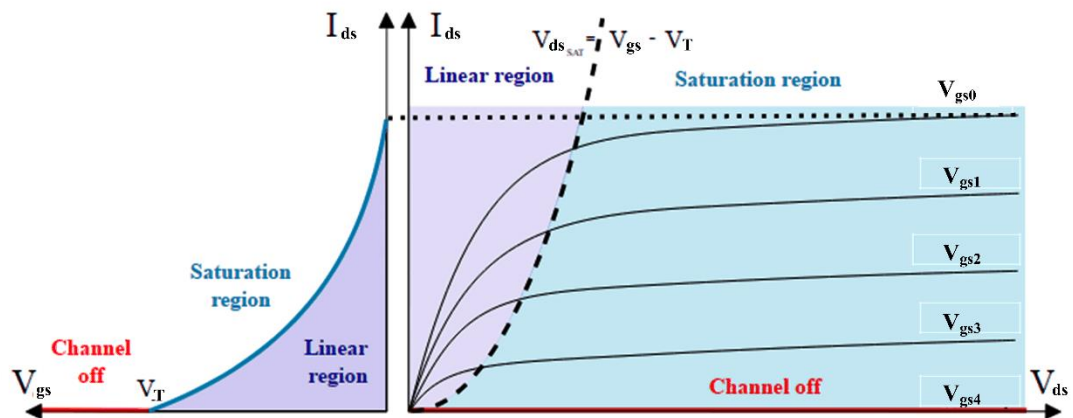


Figure 2.4: I-V characteristics and output plot of an n-channel MOSFET [79].

## 2.7 EGFET as pH sensor device

Sensitivity detection involves the measurement of changes in the surface potential between gate insulator and electrolyte. This change in surface potential modifies electric field at the insulator-semiconductor interface and modulates the channel conductance that affects drain current. The modulation of channel conductance and drain current allows the measurement of changes derived from the application of fixed source to drain voltage. Using this method, the linear plot of gate

voltage against various pH values measures unknown acidic or alkaline solutions [55]. The first ion-sensitive field effect transistor (ISFET) was invented by Bergveld in the 1970s [17]. The difference between ISFET and metal oxide semiconductor field effect transistor (MOSFET) is the presence of metal gate electrode in the latter [50], which is directly exposed to a buffer solution [55]. Silicon dioxide ( $\text{SiO}_2$ ) is the first pH-sensitive membrane to be used for the ISFET [80].

In ISFET, the adjustment of the reference electrode-source voltage (which causes the changes in the threshold voltage) leads to keep the drain-source voltage ( $V_{ds}$ ) and drain current constant. The output signal depends on the electric charge on the surface of the gate. The reference electrode voltage is constant unlike the gate voltage. The gate-source voltage ( $V_{gs}$ ) represents the electrochemical potential of the metal gate electrode which depends on the solution composition, it is the output voltage, and can be derived from the electric charge on the dielectric surface and the variation in the electrochemical potential of the gate [81]. In other words,  $V_{gs}$  can be determined from the following equation:

$$V_{gs} = V_{ref} + \Delta V \quad (2.3)$$

Where  $\Delta V$  denotes the variable potential between bulk solution and the surface of the film. Therefore, higher gate potential results in larger current passing through drain towards source of the MOSFET.

An extended gate field effect transistor (EGFET) is a structure that isolates FET from the chemical environment, in which a chemically-sensitive membrane is deposited at the end of the signal line extended from the FET gate electrode. This structure has a number of benefits, which include insensitivity to ambient light,

simple to passive packaging, flexibility of shape of the extended gate area [50] and enhanced long-term stability [82]. In addition, the EGFET structure is cost-effective, easy to fabricate, highly responsive, remarkably convenient, and very stable under light and ambient temperature. These exceptional properties make the EGFET structure ideal in the manufacture of disposable detection devices [19]. Moreover, the use of disposable membrane facilitates the exchange of sensing membrane in case of chemical damage instead of fabricating new devices [65]. The emergence of robust sensors has prompted the growing trend disposable biosensors and pH sensors in medical applications [19].

The site-binding model posits that the chemical sensitivity is dependent on the total number of surface sites per unit area ( $N_S$ ). It was put forward that larger  $N_S$  enables the ion sensing mechanism. As a result, the nanostructures with larger effective sensing areas have garnered a lot of interest in the study of pH sensing due to their high surface-to-volume ratio [83].

Metal oxide can be hydrolyzed in the presence of water forming hydroxide layers (M-OH) at its surface. The compositional water molecules in the electrolyte can be adsorbed onto the sensor surface of the scattered oxide particles. The sensor surface may then attract and adsorb additional layers of polar water molecules due to the polar hydroxyl groups (-OH). The oxide or hydroxide surface are charged by reacting with  $H^+$  or  $OH^-$  ions according to surface amphoteric reactions, which are expressed in the following two equations [84]:



where  $A$  is the surface sites,  $B$  refers to the bulk.

The above two equations can be rewritten depending on the charging of an oxide or hydroxide surface ( $M-OH$ ) with  $H^+$  or  $OH^-$  ions ( $M$  refers to metal atoms), as in the following two equations [85]:



In an acidic environment (high amount of  $H^+$  and less pH value), hydroxide sensor surface adsorbs protons [ $H^+$ ] to generate positive charges on the surface ( $M-OH_2^+$ ). On the contrary, in a basic setting (high amount of  $OH^-$  and high pH value), the surface discharges protons to produce negative charges on the surface ( $M-O^-$ ). The sensing process depends on these sites and surface charges, which are controlled by the pH of the solution (i.e., the number of protons in an electrolyte) [85]. For an extended gate of the MOSFET, the accumulation of positive charges expands the conduction channel (drain and source), which in turn increases the current flow through the channel.

There are two regimes in the pH sensing process (saturation and linear). In the saturation regime, the current decreases with higher pH values as the environment changes from acid, which supplies the gate with positive voltages to base which supplies the gate with negative voltage. In a linear regime, the threshold voltage shifts to the right for higher pH values. i.e., the positive charge accumulated at the gate at low pH value lowers the threshold voltage of the EGFET. This relation is expressed by equation (2.1).

The sensitivity parameter  $\beta$  can be estimated using the equation expressed below [77]:

$$\beta = \frac{2q^2 N_s \sqrt{\left(\frac{K_a}{K_b}\right)}}{kT C_{DL}} \quad (2.8)$$

where  $q$  is the electron charge,  $N_s$  indicates the surface site density,  $K_a$  and  $K_b$  refer to acidic and basic constants, respectively,  $k$  denotes the Boltzmann constant,  $T$  is the absolute temperature and  $C_{DL}$  describes the capacitance of the electrical double layer.

The membrane sensitivity is dependent on the charge of the surface potential voltage ( $\psi$ ) between the sensing layer and the electrolyte interface. This is based on the site binding theory [84], which posits that the number of binding sites present in the sensing membrane can change the surface potential voltage between the sensing layer and the electrolyte interface [77]. The surface potential voltage can be explained by [77]:

$$\psi = 2.303 \frac{kT}{q} \frac{\beta}{\beta + 1} (pH_{PZC} - pH) \quad (2.9)$$

where  $pH_{PZC}$  refers to the  $pH$  value at the point of zero charge. As derived from equations 2.8 and 2.9, the sensitivity parameter  $\beta$  relates directly to  $N_s$  and the linear response between  $\psi$  and  $pH$  value [77].

As shown in Figure 2.5, the  $pH$  sensing mechanism entails the reaction between the sensor surface and electrolyte. The  $pH$  sensor signified as metal oxide, is controlled by the location of surface sites which can undergo protonation or deprotonation. The sensing mechanism depends on ion adsorption, which is achieved